VOLUME 1

Perspectives of nonlinear dynamics

E. ATLEE JACKSON

CAMBRIDGE
UNIVERSITY PRESS

Exercise 7.4 What can (must?) occur to the two two-dimensional manifolds W_s^-, W_u^+ of a *stable*-node saddle (−) and a coexisting *unstable*-node saddle (+)?

A more dynamic 'interaction' is illustrated in Fig. 7.14, where a saddle-node (SN) is joined with a spiral-in saddle. The unstable manifold, $W_u(SN)$, is mostly (except for one orbit) 'thrown away' by the spiral-in saddle, S^-.

Fig. 7.14

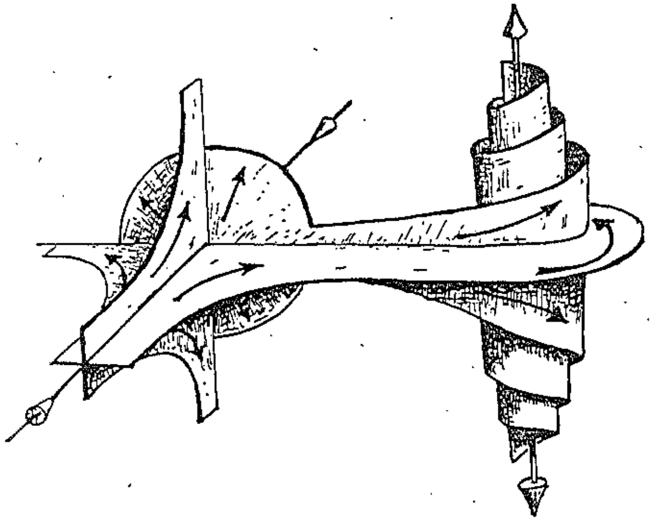

We end these illustrations with the case of two saddle-spirals, one in, the other out (Fig. 7.15). Now both the stable manifold, $W_s(S^-)$ and the unstable manifold, $W_u(S^+)$, have a spiral structure. Three other manifolds, which are asymptotic to orthogonal directions, are shown in one of these spirals, so $W_s(S^-)$ is seen with three interspersed manifolds. A similar construction could be made about the other spiral-saddle, but this figure is sufficiently complicated! The purpose of introducing these interspersed manifolds will become clear in the discussion of the Lorenz model, where it is necessary to consider such structures.

7.3 The Lorenz model

In 1963 E.N. Lorenz published a study of a highly simplified model of a particular hydrodynamic flow problem, which has become a classic in the area of nonlinear dynamics. The importance of this model is not that it quantitatively describes the

Fig. 7.15

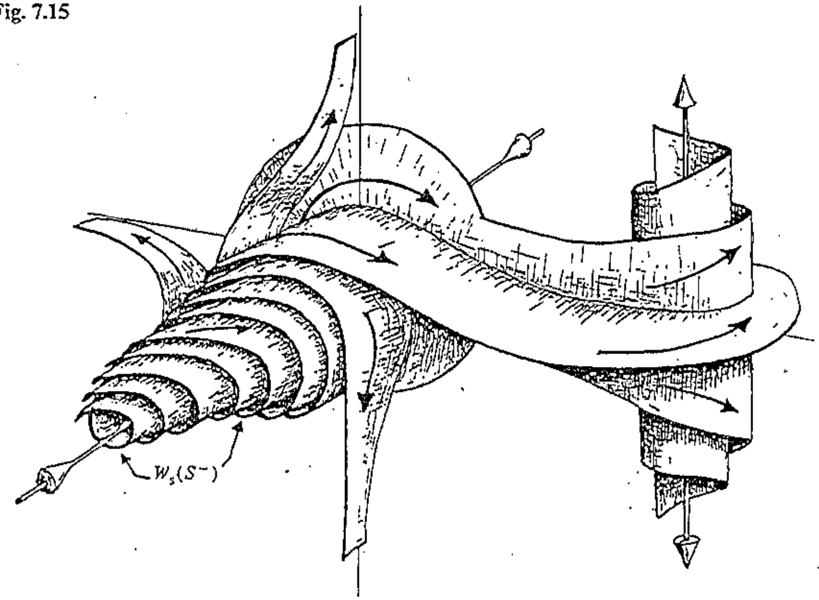

S^+: Spiral-out saddle S^-: Spiral-in saddle

hydrodynamic motion, but rather that it illustrates how a simple model can produce very rich and varied forms of dynamics, depending on the value of a parameter in the equations. Moreover, Lorenz analyzed the dynamics by employing a new type of 'map', distinct from the Poincaré map, which gives very convincing evidence that the dynamics can have a 'strange attractor' character. Since his initial study, which was followed by a long period of neglect, he and many other investigators have uncovered a rich variety of additional dynamic features in this 'simple' model, which clearly justifies its consideration in some detail.

As Lorenz later recounted (1979), this model resulted from his interest, as a meterologist, to obtain aperiodic solutions of a thermal conduction situation in viscous hydrodynamics, which could be used to simulate 'statistical' wheather conditions. Using a twelve variable system, a group at MIT numerically found solutions which indeed were not only aperiodic, but also proved to be very sensitive to the initial conditions. That is, it was discovered accidentally that solutions with nearly the same initial conditions can behave very differently after some time. Lorenz recognized that if the real atmosphere behaves like this model, then long-range forecasting of detailed weather conditions would be impossible (although he was quite cautious about what 'long-range' really meant). This group at MIT failed, however, to reduce this model to a more manageable size than the twelve variables they had used. A break in this problem came from an interaction with B. Saltzman, who had been studying thermal convection with a system of seven ordinary differential equations. Saltzman (1962) had found some solutions which were also aperiodic, and moreover four of the seven variables appeared to tend to zero in these solutions. Lorenz then sought to find such aperiodic solutions using the equations which only involve the remaining three variables. Thus was born the Lorenz model.

The approximations of the hydrodynamic equations which give rise to this model are indeed severe, and have caused many questions to be raised about the relationship of the model and real hydrodynamic flows. We will simply present the approximations which yield the model, without any implication that the hydrodynamic conduction is accurately represented by such a model (more refined models will be discussed later). It is noteworthy, however, that there are mechanical and electrical systems which are accurately represented by the Lorenz model, as will be discussed later.

The original problem, considered by Rayleigh in 1916, concerns the energy transported through a fluid layer of depth H, when the lower surface is maintained at a temperature ΔT above the upper surface.* The governing hydrodynamic equations can be written in the form used by Saltzman (1962),

$$\frac{\partial}{\partial t}\nabla^2\psi + \frac{\partial(\psi, \nabla^2\psi)}{\partial(x,z)} - \nu\nabla^4\psi - g\alpha\frac{\partial\theta}{\partial x} = 0$$

$$\frac{\partial\theta}{\partial t} + \frac{\partial(\psi,\theta)}{\partial(x,z)} - \frac{\Delta T}{H}\frac{\partial\psi}{\partial x} - \kappa\nabla^2\theta = 0 \qquad (7.3.1)$$

where it is assumed that the flow is only a function of x, z, and t (see Fig. 7.16). The function ψ is the stream function, so that the components of the flow velocity are given by

$$u_x = -\partial\psi/\partial z, \qquad u_z = \partial\psi/\partial x. \qquad (7.3.2)$$

θ is the departure of the temperature in the fluid from that which occurs when there is no convection present (i.e., $\theta = T - T_0 - \Delta T(1 - z/H)$). The constants $g, \alpha = -\rho^{-1}(d\rho/dT), \nu$, and κ represent, respectively, the acceleration of gravity, the coefficient of thermal expansion, the kinematic viscosity, and the thermal conductivity. Finally,

$$\nabla^4 \equiv \frac{\partial^4}{\partial x^4} + \frac{\partial^4}{\partial z^4} \qquad \text{and} \qquad \frac{\partial(A,B)}{\partial(x,z)} = \frac{\partial A}{\partial x}\frac{\partial B}{\partial z} - \frac{\partial A}{\partial z}\frac{\partial B}{\partial x}.$$

*See M. Velarde (in *Fluid Dynamics*, R. Balian and J.L. Peube (eds.), 1977) for a nice discussion, and some critical comments on the Rayleigh–Bénard instability.

As the temperature difference, ΔT, is increased, the transport of energy from the lower to upper surface by heat conduction becomes unstable, and is augmented by fluid convection, in the form of rolls illustrated in Fig. 7.16. Rayleigh found that this fluid motion represented by the functions

$$\psi = \psi_0 \sin(\pi a x/H)\sin(\pi z/H)$$

$$\theta = \theta_0 \cos(\pi a x/H)\sin(\pi z/H) \qquad (7.3.3)$$

would develop if the following inequality is satisfied,

$$R \equiv g\alpha H^3 \Delta T/\nu\kappa > R_c \equiv (\pi^4/a^2)(1+a^2)^3. \qquad (7.3.4)$$

Here a is related to the size of the rolls in the x direction (see Fig. 7.16), and the minimum critical value of R_c is $27\pi^4/4$, which occurs when $a^2 = \frac{1}{2}$. R is now known as the *Rayleigh number*.

Fig. 7.16

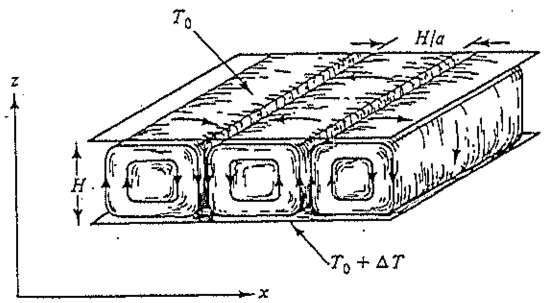

If ΔT is further increased, the Rayleigh convection solution becomes unstable, and is replaced by the time dependent dynamics studied by Saltzman. Of the seven spatial Fourier modes which he considered, the three that appeared to persist in the aperiodic solutions, and therefore were retained by Lorenz, are

$$\psi = x(t)\frac{2^{1/2}(1+a^2)}{a^2}\sin(\pi a x/H)\sin(\pi z/H)$$

$$\theta = y(t)\frac{2^{1/2}R_c}{\pi R}\cos(\pi a x/H)\sin(\pi z/H) - z(t)\frac{R_c}{\pi R}\sin(2\pi z/H) \qquad (7.3.5)$$

which now define the three functions of time, $x(t)$, $y(t)$ and $z(t)$. It should be noted that these functions have nothing to do with the spatial coordinates. The above solution differs from Rayleigh's spatial form only in the last term of θ, which thereby involves another vertical temperature variation, now containing one full wave length. Substituting the ansatz (7.3.5) into the governing equations, (7.3.1), and simply neglecting the spatial variations which are orthogonal to the ansatz (7.3.5), Lorenz obtained the system of equations (the *Lorenz model*)

$$\boxed{\begin{aligned} \dot{x} &= -\sigma(x-y) \\ \dot{y} &= rx - y - xz \\ \dot{z} &= -bz + xy \end{aligned}} \tag{7.3.6}$$

where the dot refers to the dimensionless time $\tau = \pi^2(1+a^2)\kappa t/H^2$, $r = R/R_c$, $\sigma = \nu/\kappa$ (the Prandtl number), and $b = 4/(1+a^2)$. Following Saltzman, Lorenz used the values $\sigma = 10$, and $a^2 = \frac{1}{2}$ (so $b = \frac{8}{3}$), which gives the minimum critical Rayleigh number. We will refer to these values as the 'canonical case', because they have been so widely used.

When $r < 1$, the only fixed point of the system (7.3.6) is $x = y = z = 0$, which physically corresponds to no convection (the energy is transported only by conduction). The linear motion about this fixed point has characteristic exponents given by the roots of the characteristic equation

$$(\lambda + b)[(\lambda^2 + (\sigma+1)\lambda + \sigma(1-r)] = 0 \tag{7.3.7}$$

which has three real roots if $r > 0$. If $r < 1$ they are all negative, so the heat conduction is stable, but one root becomes positive if $r > 1$, which corresponds to Rayleigh's instability. Thus the condition for the onset of convection in the Lorenz model is the same as Rayleigh's result for the full system of hydrodynamic equations.

Exercise 7.5 In the case $r < 1$, obtain a Lyapanov function for the Lorenz system, and thereby prove global asymptotic stability of the origin.

Exercise 7.6 Show that the characteristic eigenvectors at the origin can be taken to be $(0, 1, 1)$, $(\sigma, \sigma + \lambda_+, 0)$, and $(\sigma, \sigma + \lambda_-, 0)$, corresponding to the eigenvalues $\lambda = -b$, and $\lambda_\pm = \frac{1}{2}\{-(1+\sigma) \pm [(1+\sigma)^2 - 4\sigma(1-r)]^{1/2}\}$. From this, determine the variation of both the stable and unstable eigenvectors in the (x, y) plane, as r is varied from 1 to 100, by determining their angle with the x axis: Obtain the equations of motion for (s, u, z), where $s = (\sigma + \lambda_\pm)x - \sigma y$ and $u = -(\sigma + \lambda_-)x + \sigma y$, and see how these variables vary due to the z coupling. Note that the z-axis is globally contained in the stable manifold of the origin.

In addition to the origin becoming unstable when $r > 1$, the Lorenz system simultaneously acquires two additional fixed points, which we will designate as C^+ and C^-

$$(C^+, C^-): x = y = \pm[b(r-1)]^{1/2}, \qquad z = (r-1)$$

Notice that, as r increases from unity, these two fixed points move away from the remaining (unstable) fixed point at the origin. These new fixed points represent steady (time independent) fluid convection, as well as a deviation of the temperature away from a simple linear spatial dependence. The fluid convection at these two fixed points differs only in the sense of the rotation of the vortex cylinders, as illustrated in Fig. 7.17.

Fig. 7.17

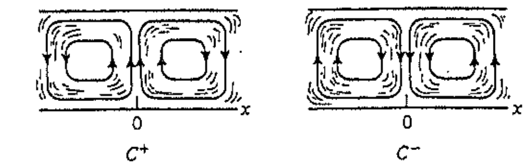

The physical system is, of course, symmetric with respect to these two situations, which is reflected in the invariance of the Lorenz equations to the transformation $(x, y, z) \to (-x, -y, z)$. The phase portrait of the equations (7.3.6) therefore always exhibits this symmetry, for all values of r.

The characteristic equation for perturbations away from the fixed points C^+ and C^- is

$$\lambda^3 + (\sigma + b + 1)\lambda^2 + (r + \sigma)b\lambda + 2\sigma b(r-1) = 0 \tag{7.3.8}$$

and it is understood that $r > 1$. Since the coefficients of (7.3.8) are real and positive, one root must be real and negative. We will call it $\lambda_0 < 0$. The other two roots are real only if $A^3 + B^2 \leqslant 0$, where

$$A = \tfrac{1}{3}b(r+\sigma) - \tfrac{1}{9}(\sigma + b + 1)^2 \qquad \text{and} \qquad B = \tfrac{1}{6}b(r+\sigma)(\sigma+b+1) - \sigma b(r-1).$$

For the canonical values $\sigma = 10$, and $b = \frac{8}{3}$, this shows that all of the roots associated with C^+ and C^- are real if

$$r < 1.34561\cdots \equiv r^*, \tag{7.3.9}$$

and they must all be negative (again because the coefficients in (7.3.8) are all positive). Thus, for $r < r^*$, any small perturbation about C^+ or C^- damps out without any oscillations.

Exercise 7.7 Obtain the characteristic equation (7.3.8) and determine the real roots for $r = 1.05$, 1.1, 1.2, 1.3, and 1.3456.

If r is slightly above r^*, there is one real and two complex conjugate roots of (7.3.8). In this case the characteristic equation can be written in the form

$$(\lambda - \lambda_0)(\lambda - \lambda_r - i\lambda_i)(\lambda - \lambda_r + i\lambda_i) = 0$$

which, when compared with the form (7.3.8), yields the relations

$$(\sigma+b+1) = -\lambda_0 - 2\lambda_r;\ b(r+\sigma) = \lambda_r^2 + \lambda_i^2 + 2\lambda_0\lambda_r$$
$$2\sigma b(r-1) = -\lambda_0(\lambda_r^2+\lambda_i^2) \qquad (7.3.10)$$

For small r, the real parts are negative, and the fixed points C^+ and C^- remain stable ($\lambda_r < 0$) as r is increased until there are roots with $\lambda_r = 0$, at some $r \equiv r_t$. Using the last expression, we readily find that this critical value of r is given by

$$r_t = \sigma(\sigma+b+3)/(\sigma-b-1). \qquad (7.3.11)$$

Exercise 7.8 Obtain λ_0 and an eigenvector at C^+ associated with λ_0 when (7.3.11) holds. The inset of C^+ (those points which tend to C^+) becomes tangent to this vector at C^+.

Note that, since r_t must be greater than one, this instability can only occur if $\sigma > b+1$ (as in the canonical case). For $r > r_t$, all fixed points are unstable, and Lorenz concluded that $r = r_t$ is the critical value of r for the instability of the steady convection (7.3.5). While this conclusion is correct for infinitesimal perturbations, it does not give any indication of the global flow pattern in the phase space. It will be shown later that, indeed, there are important *global bifurcations* which occur for $r < r_t$, and these are characteristically not detected by considering only the stability properties of the fixed points.

Fig. 7.18 (after G. Francis) summarizes the bifurcations associated with the change in stability of the fixed points, as r is increased from $r = 0$ to $r > r_t$. It is important to emphasize that the figure does not contain (nor imply) any information about global bifurcations or the global connection of these local flows. This subject will be discussed in Section 7.6.

Fig. 7.18

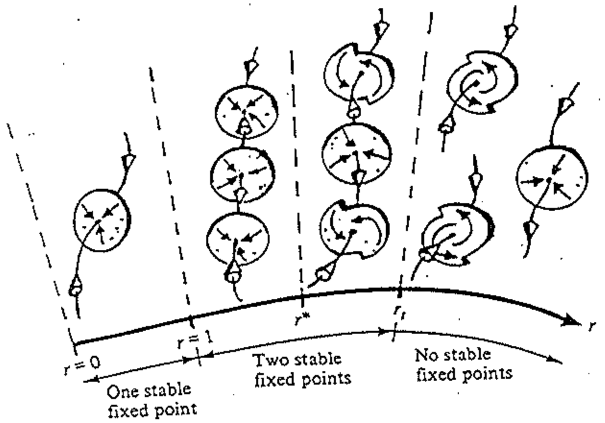

Before considering any details of the dynamics which has been obtained by Lorenz and others, we will first note two general global properties of the dynamics established by Lorenz:

Property P1 *All volume elements contract in the Lorenz flow.*

This follows (recall the proof of the general Liouville theorem) from the fact that the divergence of the velocity vector in phase space is everywhere negative. That is

$$\nabla\cdot\mathbf{v} \equiv \frac{\partial}{\partial x}(\dot{x}) + \frac{\partial}{\partial y}(\dot{y}) + \frac{\partial}{\partial z}(\dot{z}) = -\sigma - 1 - b < 0. \qquad (7.3.12)$$

Note also that this contraction is uniform in the phase space, since it does not depend on x, y, or z.

Property P2 *All solutions of the Lorenz system remain bounded in phase space for all times.*

To show this, let $u = z - r - \sigma$, so that the equations in (x, y, u) are

$$\dot{x} = -\sigma(x-y); \qquad \dot{y} = -y - x(u+\sigma); \qquad \dot{u} = -b(u+r+\sigma) + xy.$$

Then we readily find that

$$\frac{1}{2}\frac{\mathrm{d}}{\mathrm{d}t}(x^2+y^2+u^2) = -\sigma x^2 - y^2 - b(u+\tfrac{1}{2}(r+\sigma))^2 + \tfrac{1}{4}b(r+\sigma)^2.$$

Since the right side is negative everywhere outside of an ellipsoid in phase space, shown in Fig. 7.19, it follows that the distance, $s \equiv [x^2+y^2+u^2]^{1/2}$, decreases for all states outside a sphere which contains this ellipsoid (also illustrated). Therefore all states are asymptotic to this spherical region as t goes to infinity.

While a systematic approach to the general dynamics might suggest that we now consider the global aspects of the Lorenz flow, even below the critical value where all the fixed points become unstable, $r = r_t$, we will instead first follow the historical discovery of Lorenz, and consider the dynamics which he discovered when r is greater than r_t. Later, we will return to discuss the global bifurcation which occurs for $r < r_t$.

7.4 Lorenz chaotic dynamics

For the canonical values, $\sigma = 10$, and $b = \frac{8}{3}$, the critical value of r at which the time independent solutions become unstable, (7.3.11), is

$$r_t = 24.7368\ldots.$$

In his computations, Lorenz used the somewhat supercritical value $r = 28$. The

Fig. 7.19

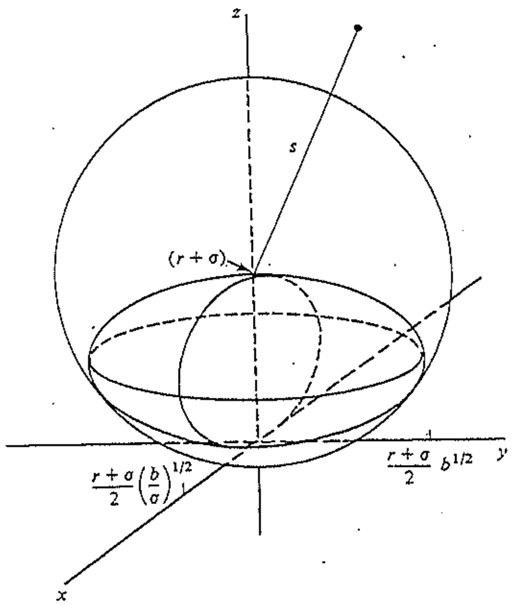

aperiodic behavior of the dynamics he found is illustrated in Fig. 7.20, which shows $y(t)$ over 3,000 iterations

In this form, the results are simply complicated, and not particularly interesting (except, of course, for somebody looking for complications!). The dynamics, shown in Fig. 7.21, is more revealing, but actually appears deceptively simple. The motion has been projected onto the (x, y) and (z, y) planes, for the case where the initial condition is $(0, 1, 0)$. The points (C^+, C^-) are the fixed points $(6 \times 2^{1/2}, 6 \times 2^{1/2}, 27)$ and $(-6 \times 2^{1/2}, -6 \times 2^{1/2}, 27)$, which indicates the scale in the figures.

It will be noted that the dynamics now takes the system in a growing spiral away from one C-point, then it drops into the neighborhood of the other C-point, and proceeds to spiral away from it also (recall that the unstable manifold of the C-points is two dimensional). Thus the dynamics flip-flops between the neighborhood of these two fixed points. Physically, this would presumably mean that the vortical cylinders

Fig. 7.20

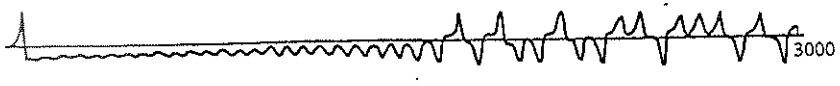

Fig. 7.21

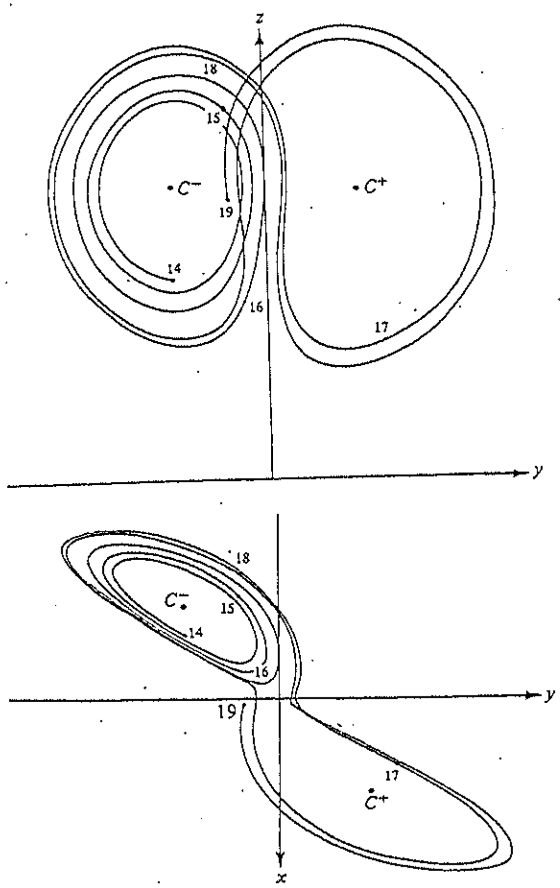

change both their rate of rotation in an increasingly oscillatory manner in time, and then completely reverse their sense of rotation to a relatively stationary state, and then increasing oscillate their rotation rate once again.

As shown above (Property P1), the flows in the phase space uniformly contract, so that the volume into which the trajectories tend must be zero (when based on the usual three-dimensional measures – more details are in Appendix B and below). This suggests that the trajectories tend asymptotically to some two-dimensional surface in the phase space. The approximate nature of this 'surface' was illustrated by Lorenz in Fig. 7.22. This surface has a 'butterfly' structure, with its wings going in and out

Fig. 7.22

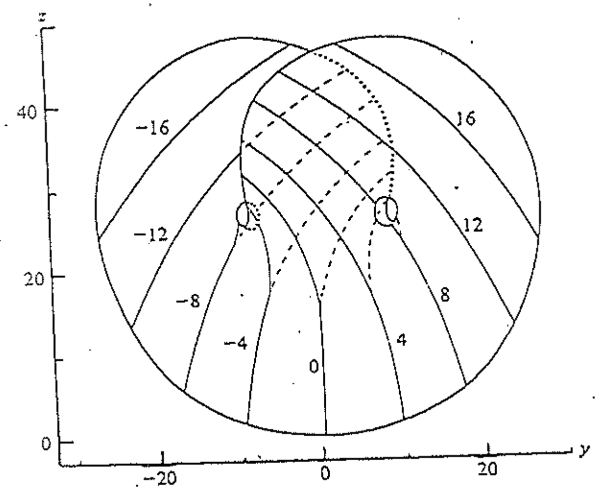

of the (y, z) plane of the figure. The lines with numbers indicate the intersection of this surface with planes of constant x values, corresponding to these numbers.

With improvements in computer graphics, other representations of this asymptotic 'surface' have been published, notably Fig. 7.23 obtained by Lanford (1977). Here the solution starts near $(0, 0, 0)$ and moves out along the unstable direction, and loops immediately to the neighborhood of C^-, spirals outwards, then flips over to the region of C^+, to spiral outward again. The trajectory below the plane $z = r - 1 = 27$, which contains C^+ and C^-, is represented by the dotted curves. Lorenz recognized that this asymptotic set (the ω-limit set) cannot simply be a surface, if the trajectory continues to spiral, because the continual spiraling of the trajectories alternately about the points C^+ and C^- makes it impossible for any trajectory to lie on a surface (because it would have to be self-intersecting, and hence not unique). He described this asymptotic set as an 'infinite complex of surfaces', but it is now referred to as a fractal set, since it has a dimension (capacity) between two and three (Russel *et al.* (1980) and Lorenz (1984) have obtained $d_c = 2.06 \pm 0.01$).

As nice as the above graphics may be, they do not really establish the complexity of this limiting set of points (the ω-limit set) of the trajectories. In particular, there is nothing in these results which rules out the possibility that the trajectories might ultimately settle down to some limit cycle in the phase space. What Lorenz did after finding the above results, was to introduce a new type of 'map', generated by the dynamics, and to show, with the help of this 'map', that such stable limit cycles most likely do not exist for his value of r. His result, which again depends on numerical

Fig. 7.23

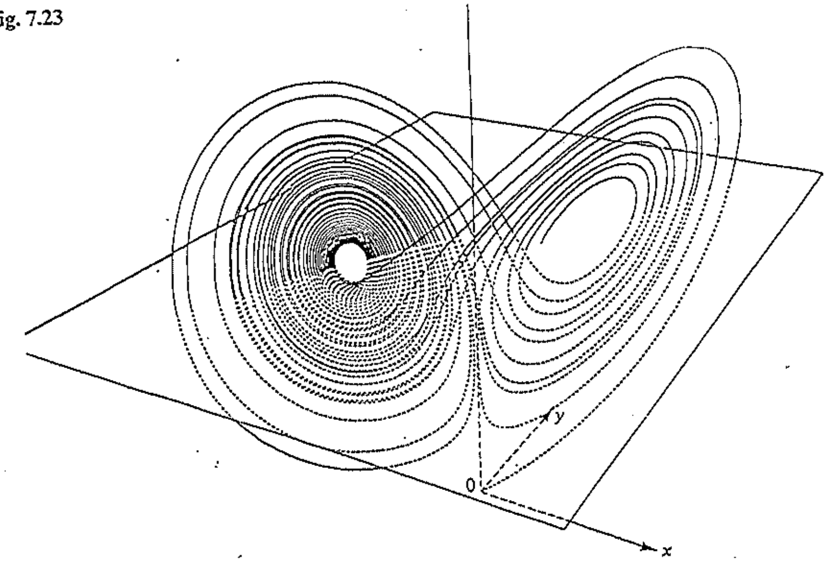

computations, is not a mathematical proof, but nonetheless is a very convincing and very imaginative approach to this question. While Lorenz now (1979) refers to this 'map' as a 'form of Poincaré map', it is quite distinct from what Poincaré suggested, and has moreover stimulated other variants of this *Lorenz map*, which have further enlightened our understanding of complex dynamical situations.

To make this point clear, we should recognize from the outset that Lorenz's approach to the investigation of the dynamics does not introduce a real map, as in Poincaré's method, because, to the value of some variable, x_k, it does not associate a unique value of this (or any other) variable, x_l. Instead, Lorenz introduced what we will call a *match*, to distinguish it from a map.

When some given conditions, $Q(x, \dot{x}) \geqslant 0$, are satisfied, a *match* associates with each value of some dynamic variable, x_k, the set of values, $\{x_l\}$, which x_l acquires when the condition is satisfied the next time. Thus a match is a one-to-many association between these variables x_k and x_l, $M(Q, k, l)$.

This concept of a match is presumably most useful when the set of values, $\{x_l\}$, is not very 'scattered', so that the match can be approximated by a smooth functional relationship, $x_l(n+1) \simeq F(x_k(n))$, as in Fig. 7.24. If, moreover, the approximating function $F(x_k)$ is unique, as in the second figure, then the match is essentially the same as a map (the nonunique case will be discussed below). In the case of the Poincaré map, the uniqueness and continuity of the function is guaranteed by the

Fig. 7.24

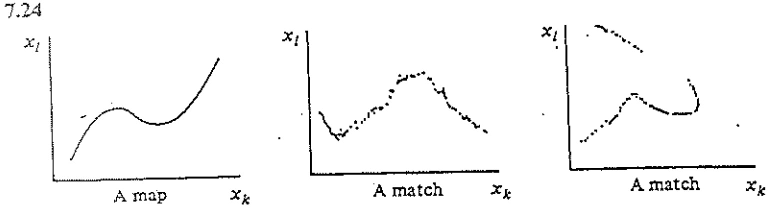

uniqueness of the dynamics, and by the restrictive conditions which define the map (which were carefully discussed by Birkhoff (1922)). This uniqueness and the continuity may not be retained in a match, because the conditions, $Q(x, \dot{x}) \geqslant 0$, may not be sufficiently restrictive.

This point is made clear by considering Lorenz's original match. He considered the association of the values of $z(t)$, when it is a maximum (i.e., $\{Q | \dot{z}(t) = 0, z > r\}$), and its value the next time it is a maximum. If we let M_n represent the nth maximum value of $z(t)$, then he considered the association of M_{n+1} with M_n.

His motivation for considering such a strange association was expressed by him as follows (Lorenz, 1963):

> . . . we find that the trajectory apparently leaves one spiral only after exceeding some critical distance from the center. . . . Moreover, the extent to which this distance is exceeded appears to determine the point at which the next spiral is entered, this in turn seems to determine the number of circuits to be executed before changing spirals again. It therefore seems that some single feature of a given circuit should predict the same feature of the following circuit. A suitable feature of this sort is the maximum value of z. . . .

The new feature here is that he is suggesting that this complicated motion may have a predictive (i.e., nearly unique) association in only a 'single feature'. The motion, after all, is in a three-dimensional phase space, so that any Poincaré map (which is unique) must associate two features at one time with their values at another time, rather than a single feature. However, Lorenz's conjecture proved to be warranted, as is shown in his following justifiably famous feature relating M_{n+1} to M_n: Fig. 7.25 clearly shows that there is essentially a smooth functional relationship connecting the values M_{n+1} and M_n. Moreover, Lorenz noted that an essential feature of the above curve is that it has a slope whose magnitude exceeds unity everywhere. The important consequence of this is that all periodic trajectories of this system must be unstable, as we saw in Chapter 4. Therefore the ω-limit set of this system cannot be a limit cycle, at least for the value of r used by Lorenz. This, of course, can change if r is changed, and in fact limit cycles do occur at larger values of r, as will be discussed later. The fine structure of the Lorenz match has been studied by Richtmyer (1986). The above conclusions of course depend on the assumption that Lorenz's

Fig. 7.25

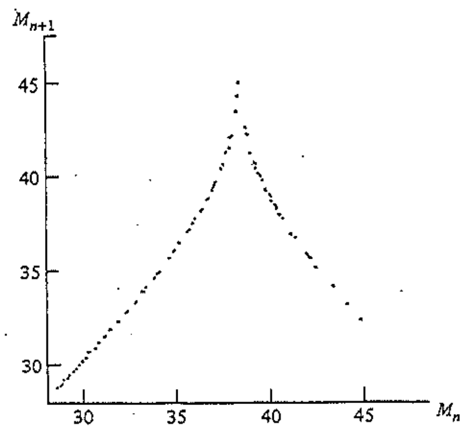

match is sufficiently smooth to be treated as a map. By way of comparison, see the Rössler 'maps' in section 7.11.

Lorenz therefore established that, when $r = 28$, the trajectories converge into a region of phase space which has zero volume (based on the usual three-dimensional measure) and yet, within the approximation inherent in his match, appears to contain no stable fixed points nor stable limit cycles. Such a ω-limit set can be reasonably called a *strange attractor*, because it also possesses the property of being *sensitive to initial conditions* (what Lorenz referred to as 'the instability of nonperiodic solutions . . . in the sense that solutions temporarily approximating it do not continue to do so.') This was a major discovery, and would be sufficient to warrant the interest in the Lorenz system, but there are many other interesting features to be discovered. Before discussing these features, we will consider several other examples of physical systems which are associated with the Lorenz equations

7.5 A 'Lorenz-dynamic' fluid system

In the derivation of the Lorenz equations for the case of Rayleigh–Bénard convection, a number of severe approximations were used, whose nature and validity are hard to assess. Before proceeding to analyze further the dynamics of the Lorenz equations, we will consider a simpler system, in which it is possible to specify clearly the approximations, because its dynamics is sufficiently restricted by boundary constraints (Yorke and Yorke, 1979).

The system (Fig. 7.26) consists of a fluid in a circular tube, which stands vertically in a gravitational field. The tube has mean radius R, and a small cross-sectional area,

Fig. 7.26

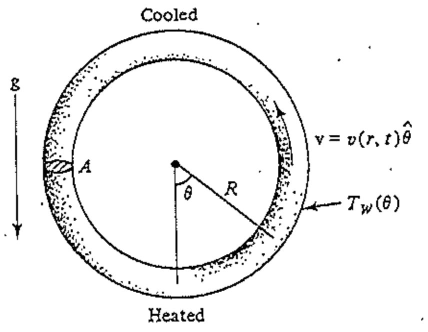

A. The only approximation which we require is that the fluid velocity can taken to be $\mathbf{v}(r, \theta, t) = v(r, t)\hat{\theta}$. This means that, in the convective aspects of the dynamics, the fluid is treated as incompressible. The wall of the tube is maintained at a constant temperature, $T_W(\theta)$, which is an arbitrary function of θ. The fluid density depends on its temperature, $T(\theta, t)$,

$$\rho = \rho_0[1 + \alpha(T_0(t) - T(\theta, t))],$$

where $\alpha (>0)$ is the coefficient of thermal expansion and $T_0(t)$ is its mean temperature, $\int_0^{2\pi} T(\theta, t)\, d\theta = 2\pi T_0(t)$. The heat transfer between the wall and the fluid is given by

$$K(T_W(\theta) - T(\theta, t)]$$

where K is a constant. Finally, the fluid flow is opposed by a frictional force, f, proportional to its mean flow rate

$$q(t) = \int \mathbf{v}(r, t) \cdot d\mathbf{A},$$

so that

$$F = \hat{\theta} \int \mathbf{f} \cdot d\mathbf{A} = -\mu\rho_0 q(t)\hat{\theta}$$

where μ is a constant.

The equations of motion of the fluid now reduce to

$$\rho_0 \frac{\partial \mathbf{v}}{\partial t} = -\nabla P(\theta, t) + \rho_0(1 + \alpha(T_0 - T))\mathbf{g} + \mathbf{f}$$

where we have again ignored the variation of ρ on the left side, and $P(\theta, t)$ is the pressure, $\mathbf{g} = -g \sin\theta\, \hat{\theta}$. If this is integrated by

$$\frac{1}{2\pi}\int_0^{2\pi} d\theta \int d\mathbf{A},$$

we obtain

$$\frac{dq}{dt} = \frac{Ag\alpha}{2\pi}\int_0^{2\pi} \sin\theta\, T(\theta, t)\, d\theta - \mu q(t). \tag{7.5.1}$$

The second equation we need is for the heat transfer. We will ignore the thermal conduction in the fluid (see Exercise 7.9), in which case

$$\frac{\partial T}{\partial t} + \frac{1}{AR} q(t) \frac{\partial T}{\partial \theta} = K[T_W(\theta) - T(\theta, t)]. \tag{7.5.2}$$

Now, if we expand $T_W(\theta)$ and $T(\theta, t)$ in Fourier series

$$T_W(\theta) = W_0 + \sum_{n=1}^{\infty} V_n \sin(n\theta) + W_n \cos(n\theta)$$

$$T(\theta, t) = T_0(t) + \sum_{n=1}^{\infty} S_n(t) \sin(n\theta) + C_n(t) \cos(n\theta) \tag{7.5.3}$$

the equation of motion, (7.5.1), only involves $S_1(t)$, and we obtain a closed system of only three equations from (7.5.1) and (7.5.2),

$$\begin{aligned}
\frac{dq}{dt} &= \frac{1}{2} Ag\alpha S_1(t) - \mu q(t) \\
\frac{dS_1}{dt} &= \frac{1}{AR} q(t) C(t) + K[V_1 - S_1(t)] \\
\frac{dC_1}{dt} &= \frac{1}{AR} q(t) S_1(t) + K[W_1 - C_1(t)]
\end{aligned} \tag{7.5.4}$$

the remaining equations from (7.5.2) are decoupled from these,

$$\left.\begin{aligned}
\frac{dS_n}{dt} &= \frac{n}{AR} q(t) C_n(t) + K[V_n - S_n(t)] \\
\frac{dC_n}{dt} &= -\frac{n}{AR} q(t) S_n(t) + K[W_n - C_n(t)]
\end{aligned}\right\} \quad (n > 1) \tag{7.5.5}$$

and

$$\frac{\partial T_0}{\partial t} = K[W_0 - T_0(t)]$$

The equations (7.5.4) can be put into the form of the Lorenz equations, (7.3.6), (or nearly so) by setting

$$\tau = Kt, \qquad \sigma = \mu/K, \qquad r = \gamma W_1, \qquad r' = \gamma V_1 \tag{7.5.6}$$

where $\gamma = g\alpha/2K\mu R$, and identifying

$$x(t) = q(t)/AKR, \qquad y(t) = \gamma S_1(t), \qquad z(t) = \gamma[W_1 - C_1(t)]. \qquad (7.5.7)$$

This yields

$$\frac{dx}{d\tau} = \sigma(y - x)$$
$$\frac{dy}{d\tau} = rx - y - zx + r' \qquad (7.5.8)$$
$$\frac{dz}{d\tau} = xy - z$$

which, aside from the additional constant r', is (7.3.6) with $b = 1$. The constant r' comes from an asymmetric heating of the wall, V_1 in (7.5.3). If r' is too large, relative to r, then the flow is stable in the preferred direction (depending on the sign of V_1). In the simplest situation, when $T_W(\theta) = W_0 + W_1 \cos\theta$, (7.5.3) yields decaying solutions

$$\frac{d}{dt}(S_n^2 + C_n^2) = -2K(S_n^2 + C_n^2)$$

and $T_0(t) = W_0 + \exp(-Kt)(T_0(0) - W_0)$. Therefore, in this case, as $t \to \infty$,

$$x \sim q(t), \qquad y \sim \left[T\left(\frac{\pi}{2}, t\right) - T_W\left(\frac{\pi}{2}\right)\right], \qquad z \sim [T_W(0) - T(0, t)].$$

fluid velocity	*Temperature difference midway up the side*	*Temperature difference at the bottom*

Exercise 7.9 Add the thermal conductivity term $\lambda(\partial^2 T/\partial\theta^2)(\lambda \equiv \kappa/R^2)$ to the right side of (7.5.2), and show that we can obtain (7.5.8) with modified relationships, (7.5.6), and (7.5.7). In particular, determine the influence of λ on r, and hence on the stability of the flow.

An experiment involving a fluid arrangement of a similar nature has been carried out by Creveling, Paz, Baladi, and Schoenhal (1975). The experimental arrangement was slightly different from the above theory, as illustrated in Fig. 7.27(*a*). The bottom half of the convection loop was maintained with a uniform heat flux, whereas the upper half had a constant temperature wall. Temperature reversals were observed between the two points A and B, as illustrated in Fig. 7.27(*b*). This temperature reversal is also related to a reversal in the fluid flow in the loop. The qualitative behavior is clearly the same as the above simpler situation, and they obtained more detailed agreements with the experimental results, using a suitably modified theory.

Fig. 7.27 (*a*) Free convection loop employed for experimental study ($R = 38$ cm, $r = 1.5$ cm). (*b*) Fluctuations in the temperature difference between sections A and B exhibiting reversion to original flow direction after a flow reversal.

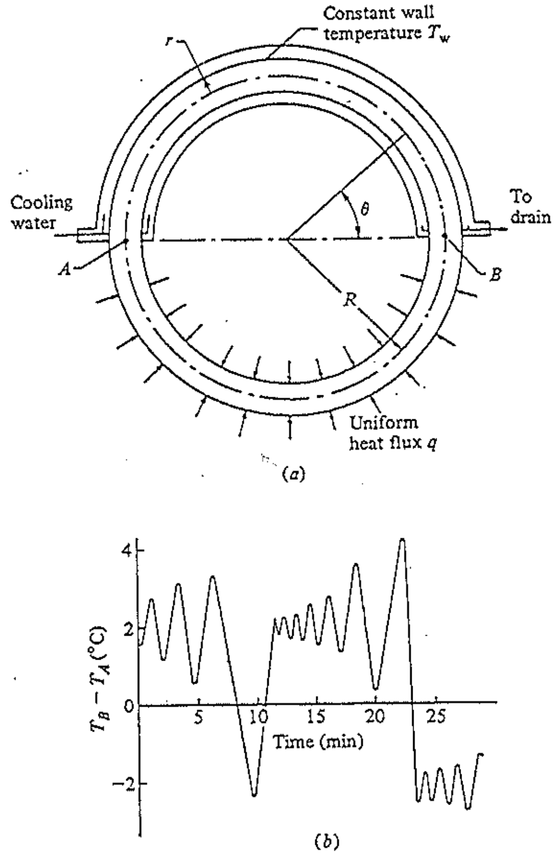

7.6 Dynamo dynamics

One of the most spectacular features of geophysical dynamics is the numerous erratic reversals of the Earth's magnetic field which have occurred over at least the last 150